Simulation of two-dimensional Kerr photonic crystals via fast Fourier factorization

J. J. Bonnefois, Géraldine Guida, and Alain Priou

GEA, IUT de Ville d'Avray, Université Paris X, Ville d'Avray 92410, France

Michel Nevière and Evgeny Popov

Institut Fresnel, UMR 6133, case 161, Faculté des Sciences et Techniques, Centre de Saint-Jerome, Marseille, France

We present an adaptation of the fast Fourier factorization method to the simulation of two-dimensional (2D) photonic crystals with a third-order nonlinearity. The algorithm and its performance are detailed and illustrated via the simulation of a Kerr 2D photonic crystal. A change in the transmission spectrum at high intensity is observed. We explain why the change does not reduce to a translation (redshift) but rather consists in a deformation and why one side of the bandgap is more suited to a switching application than the other one.   © 2006 Optical Society of America

OCIS codes: 190.0190, 190.1450, 190.3270.

1. INTRODUCTION

Photonic crystals (PCs) are dielectric materials arranged periodically. This periodicity leads to remarkable properties of the dispersion relation: Light can propagate (permitted band) or cannot propagate (forbidden band) in PCs at some frequency ranges.[1] Dispersion relation features are linked to the parameters of the PCs (lattice constant, materials). It is then possible to tailor properties of PCs by playing with these parameters. The discovery of the localized modes that occurr when a defect is inserted in the PC completed the first intuitive analogy between photons in PCs and electrons in semiconductors. Since their introduction in 1987,[2] PCs are still under intensive investigations.[3] The challenge is to perfectly control the propagation of light, a control that offers a vast implication in both quantum optics and passive optical devices. An advanced high-technology potential of PCs can be achieved with a dynamic tunability of their bandgaps. Active optical design could then be envisaged. The first basic idea was to couple PCs with materials whose optical properties change under the influence of an external stimulation. In that aim, several materials have been recently proposed (see, for instance, Ref. 4). Alternative materials presenting an electro-optic effect or temperature-induced change in the refractive index were proposed.[5,6] However, these schemes are usually rather slow compared with the time scale required for an all-optical high-speed operability for modern communications. Moreover, they do not provide tunability without an external function (as required for passive all-optical limiters, for instance). To cope with these difficulties, Kerr nonlinear materials have been suggested.[7–9] For such materials, relaxation time scales can be very short ($\tau \approx 10^{-15}$ s) and it is possible to control the optical properties of the material directly via the input optical light. In a Kerr material, the dielectric constant ϵ depends on the product of intensity and electric susceptibility $\chi^{(3)}$. Components of $\chi^{(3)}$ have weak values, and nonlinear effects usually appear only for very large values of the intensity associated with pulsed lasers. For PCs, however, the situation differs drastically because of the diffraction phenomenon. The light field can be extremely enhanced in some area inside the PC due to a low group velocity. In particular, a light field localized in the defect modes is intense,[10] leading to a lower threshold for, e.g., an optical switch. The exaltation of the field contributes to an increase in the apparent nonlinearity that can become much more important than in the bulk material.

The first numerical analyses of nonlinear photonic crystals (NPCs) have been on one-dimensional (1D) (dielectric periodic multilayers) structures.[7–9] Since these first analyses, extensive studies have adopted this geometry. The simplicity of this model (invariant in two directions) permits an analytical solution. Simulations are rapid and do not require a large storage capacity computer. Dynamical shift in the location of the bandgap,[9] existence of optical bistability in defect layers,[11–13] or even gap solitons[7,14–19] were predicted in 1D NPCs. The feasibility of all-optical limiters was also addressed.[9,20–22] However, 1D structures do not allow us to either demonstrate the existence of propagation of light without loss in a sharp bend waveguide or to eliminate guided modes in homogeneous layers. Extension of properties from a 1D model toward a two-dimensional (2D) or three-dimensional (3D) model is not so straightforward and a greater potential is expected from multidimensionality. In other words, 2D and 3D structures capture the same properties, although 3D structures provide their generalization in the whole space. Moreover, 2D PC fabrication benefits from a more mature technology than the 3D PCs. Studies that focus on 2D nonlinear structures are then of great interest and have attracted more scientists since 2000. Most studies on 2D Kerr NPCs use the Bloch-wave decomposition and are devoted to infinite structures[23] or

use the finite-difference time-domain algorithm that requires large storage and time-consuming computing.[24]

We propose in this paper a highly efficient method to deal with 2D NPCs that consist of a stack of rod gratings made of parallel nonlinear and linear cylinders embedded in a linear or nonlinear medium. This method is derived from the most recent version of the classical differential theory.[25] This method has been used recently by one of the authors[26] to study overlapping stacks of linear gratings, but also to study deep metallic gratings with grooves filled with a nonlinear material illuminated in TM polarization (H along the grooves).[27] In both cases, convergence of the numerical result turned out to be fast.

The paper is organized as follows: First we briefly describe the fast Fourier factorization (FFF) theory and process; then we show some possibilities of this tool to explore properties of 2D Kerr nonlinear PCs and propose a physical explanation of the strong modification of the transmission spectrum induced by the nonlinearity.

2. RESOLUTION OF NONLINEAR MAXWELL EQUATIONS USING THE FACTORIZATION RULES IN A TRUNCATED FOURIER BASIS: THE FAST FOURIER FACTORIZATION METHOD

The FFF method is a highly efficient differential method relying in essence on Li's factorization rules[27] that can be used to obtain both the transmission and the field map of PCs. Here we will briefly describe the theory (the interested reader can find a detailed presentation of this method in Refs. 25 and 28).

The periodic structure to model is infinite along its x axis and is illuminated by a plane wave where the k_y component is not null (see Fig. 1). All the relevant physical quantities such as the fields, permittivities, and wave vectors are described by their truncated Fourier series. Then, using the classical differential theory, we can obtain from Maxwell's equations the following matrix differential set:

$$\frac{\mathrm{d}}{\mathrm{d}y}\begin{pmatrix}[E_x]\\[E_z]\\[H_x]\\[H_z]\end{pmatrix} = M(y)\begin{pmatrix}[E_x]\\[E_z]\\[H_x]\\[H_z]\end{pmatrix}. \tag{1}$$

As this set describes the electromagnetic behavior of the diffracting object, its resolution via a shooting method should provide the transfer matrix of the structure. But this method cannot be used because it is on thick objects and numerical contamination would occur. To bypass this difficulty, a thick object has to be cut into several thin layers so that each transfer matrix can be calculated via the above method without significant contamination. Then the S-matrix propagation algorithm aggregates the results to obtain the global transfer matrix of the stack.[25]

The difference between the classical differential theory and the FFF relies on a better understanding of how to calculate the Fourier series of a product. Indeed, Laurent's rule states that the Fourier components of f and g obey $(fg)_n = \sum_{m=-\infty}^{+\infty} f_{n-m} g_m$. But this equation can become inaccurate if truncated and used on discontinuous functions such as the permittivity and the electromagnetic field. On

the contrary, the inverse rule provided by Li[27] converges rapidly if (fg) is continuous while f and g are not. This rule states that $(fg)_n^{\{N\}} = \sum_{m=-N}^{+N}(\|1/f\|^{\{N\}})^{-1}_{n,m} g_m$, where N is the truncation coefficient and $\|X\|$ is a Toeplitz matrix whose (n,m) entry is the $(n-m)$th Fourier component of X. Noticing that ϵE_x and $\langle 1/\epsilon \rangle (\partial H_z / \partial x)$ remain continuous while the object's profile is a lamellar grating allowed Li to account for a better, faster converging rigorous coupled-wave theory. However, these two quantities will not remain continuous if we are to consider arbitrary-shaped objects and so they cannot be used here for our PCs.

The FFF adds further refinement[26] as it decomposes the field upon an $(\mathbf{N}, \mathbf{T})$ basis, where $\mathbf{N}$ and $\mathbf{T}$ are vectors normal and tangential to the object's surface, respectively. It then uses the quantities E_T and ϵE_N that are continuous, the latter being treated via Li's inverse rule. This locally variable $(\mathbf{N}, \mathbf{T})$ basis allows better convergence. Here, either better convergence means faster simulations of objects that could already be simulated with other methods or it will allow us to simulate thick, strongly index-contrasted structures such as real metal mixed with dielectrics in a nontrivial geometry that were previously forbidden. The FFF method then provides a different $M(y)$ matrix to be used in Eq. (1), an $M(y)$ matrix that allows accurate results with a more severe truncation.

3. ALGORITHMIC STRUCTURE TO IMPLEMENT THE KERR EFFECT IN A PHOTONIC CRYSTAL

A permittivity map is created for the PC (see Fig. 1). One period of the PC is meshed with Q layers, each one being constituted by 2^N cells [to optimize use of the fast Fourier transform (FFT)]. For each layer, the FFF is applied and the $M(y)$ matrix in Eq. (1) is calculated. The layers are chosen thin enough that a single Runge–Kutta integration of the fourth order will be sufficient to solve Eq. (1) and that the $M(y)$ matrix can be considered constant in each layer. In fact, from a computational point of view, more layers, needing only one integration with a constant M, are preferable to fewer thicker layers, which need a subtler (and slower) integration technique because the $M(y)$ matrix can no longer be considered constant in the layer.

The field map, obtained via the S-matrix propagation algorithm, is then used to calculate the new Kerr-induced permittivity map. In each cell of the mesh, the new permittivity becomes $(\epsilon_{\text{linear}} + \chi^{(3)} |E^2|)$. A new iteration of the whole process is then done by applying the FFF on these new permittivity values. It is expected that after several such iterations, the permittivity maps will converge.
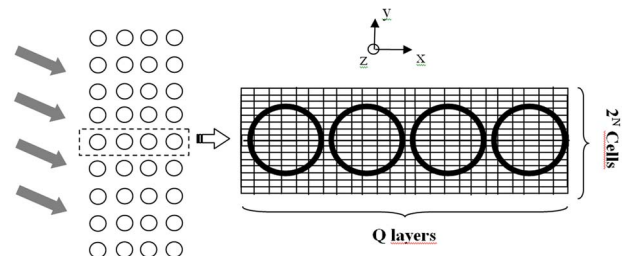

Fig. 1. Structure of the PC and mesh used for its simulation.

(a)   (b)
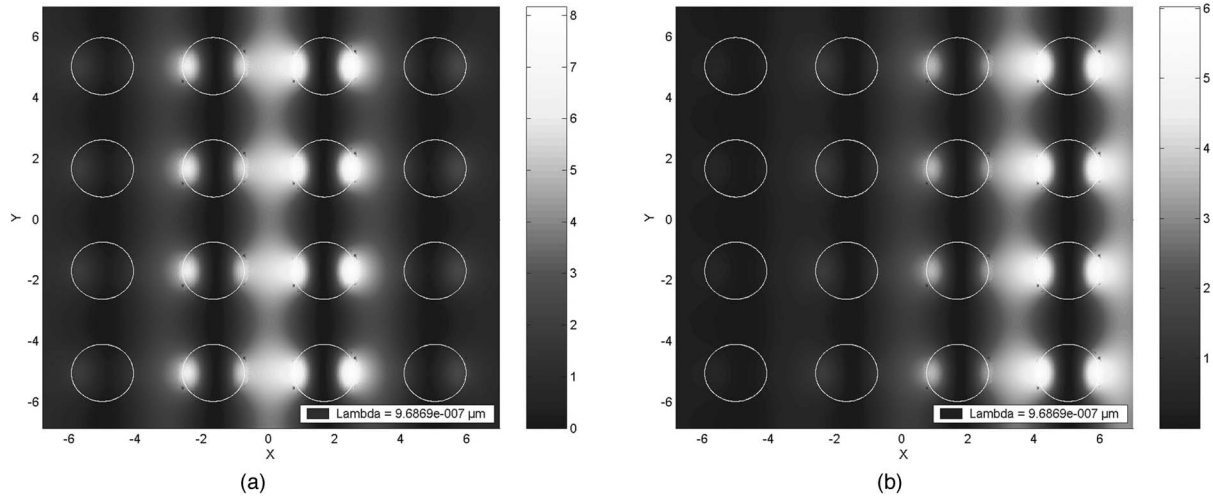
Fig. 2.   Field map at a 968 nm wavelength of our structure illuminated with intensity (a) 0.5320 and (b) 0.5321 (arbitrary units). The inhomogeneities in the rods are obvious.

In reality, convergence would have seldom happened if we had applied the above method as it is. The convergence usually needs enforcement of a slow modification of the permittivity map for each iteration. This is done by arbitrarily imposing as a new permittivity the weighted sum of the old and the new permittivities. For example, we often observed a pseudoperiodic oscillation of our algorithm toward two stable points that were numeric artifacts rather than real physical solutions.

If we consider $(U)_n$ a sequence describing the permittivity map for each nth iteration, a convergence such as $\lim_{n\to\infty} U_n = U_{\text{limit}}$ is expected, but a pseudo-convergence such as $(\lim_{n\to\infty} U_{2n} = U_{\text{limit},1}, \quad \lim_{n\to\infty} U_{2n+1} = U_{\text{limit},2}, \quad \text{with} \quad U_{\text{limit},1} \neq U_{\text{limit},2})$ where the even and odd subsequences that converge toward different limits can sometimes appear. In this case defining the sequence $(W)_n$ such as $W_{n+1} = 1/2(U_n + U_{n+1})$ and using it as the new permittivity map prevents the oscillation between two nonphysical equilibrium points $U_{\text{limit},1}$ and $U_{\text{limit},2}$. The use of such weighting can be seen as similar to the introduction of a relaxation factor to stabilize the numerical resolution of some nonlinear equations[29] and is commonly used when studying nonlinear optics.[30]

It is of interest to note that in this example we used a 50:50 ratio in the weighting but that other ratios are possible, 70:30 being the most effective if we have to trade between speed and robustness. The convergence usually occurs within less than ten iterations, except when the PC state switches between opaque and transparent.

4. RESULTS AND DISCUSSION

The FFF of the electromagnetic components permits us to obtain, among other information, the transmission versus the wavelength for 2D PCs that constitute a stack of rod gratings made of parallel circular cylinders. We will present results obtained with the geometry depicted in Fig. 1. The structure is a 336 nm period square lattice made of 94 nm radius dielectric rods with a refractive index equal to 3, standing in vacuum. There are four layers of rods as the PC is unlimited in only two directions (y
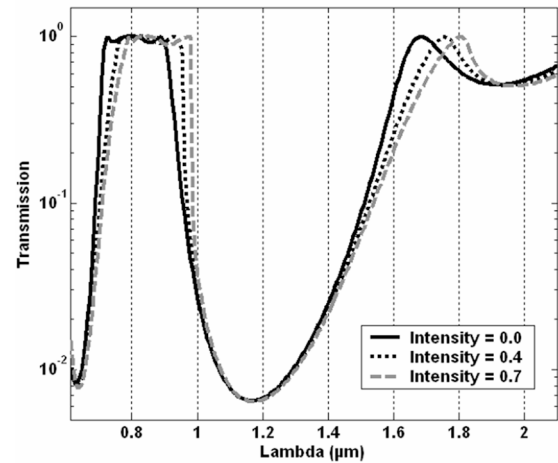

Fig. 3.   Transmission versus λ for different values of the intensity I (arbitrary units) of the incident field.

and z). We assume that the rods are made of a Kerr material. In this case, the strongly inhomogeneous electromagnetic field produces an inhomogeneous permittivity (see the example shown in Fig. 2). As a consequence, regular rigorous frequential methods[31,32] for which the rods must be homogeneous become inefficient here. The purpose of this paper is to provide information on the numerical implementation of a theory[25] that we hope would be an efficient tool for researchers.

Linear PCs as depicted in Fig. 1 have been extensively studied during the past two decades. The transmission versus λ shows a large bandgap from 0.9 to 1.6 μm.[1] Properties of these perfect structures have been widely explored numerically, so it is easy to compare our results with the literature.

Figure 3 shows the evolution of the transmission feature when the energy of the incident field increases. Actually, the permittivity varies locally as $(\epsilon_{\text{linear}} + \chi^{(3)}|E^2|)$ with $\chi^{(3)}$ being the nonlinear cubic susceptibility parameter and $|E|^2$ being proportional to the local energy. The rods are filled with a positive Kerr material ($\chi^{(3)} > 0$), i.e., the refractive index increases proportionally to the inten-

sity. At low intensity, the Kerr effect has a negligible effect on the refractive index and we find the same behavior as in linear optics. When the magnitude of the incident plane wave increases, the refractive index of the rods also increases and becomes more inhomogeneous. Following a first intuitive reasoning, we should expect a redshift of the band edges, since it is known that for a stronger index contrast, bandgaps present a shift toward larger wavelengths.[1] The direct study of the transmission versus λ permits us to clearly reveal the shift of the band edges. But there is more than a uniform shift here: Contrary to a theoretical experience in which all the rods' index would increase, here only the illuminated rods are affected by the Kerr effect. As a consequence, at the bottom of the bandgap, where the PC is totally reflective, the light cannot penetrate inside the PC and no Kerr effect occurs. Thus increasing the incoming intensity leaves unchanged the bottom position of the bandgap transmission. On the contrary, when the PC is transparent, all the rods are illuminated and we observe the expected redshift. At the edges of the bandgap, as the PC is neither totally reflective nor transparent, only the first layers of the cylinders are illuminated by the incident wave while the deeply burrowed layers remain in the dark, unaffected by the Kerr effect. We then have a partial redshift due to the modification of the index of the superficial layers.

It is then of interest to note that the blue edge and the red edge of the bandgap do not behave in the same way while illuminated. On the blue edge of the gap, the superficial layer shifts from opaque to transparent while illuminated, allowing the following layer to be illuminated and become in turn transparent. This process continues until the whole stack of layers in the PC have switched from opaque to transparent. We then have on the blue side of the gap an abrupt change of transparency with a very steep slope, becoming steeper while the incoming intensity increases. On the contrary, the PC switches from transparent to opaque on the red side of the bandgap while the incoming intensity increases. As a consequence, the deeply burrowed rods that were illuminated in the transparent state are deprived of energy as the superficial layers become reflective. As a consequence, those burrowed layers become unaffected by the Kerr effect. Unlike on the blue edge of the bandgap where the switching from opaque to transparent of the superficial layers triggers the illumination and switching of the whole stack of layers, on the red side of the bandgap the switching from transparent to opaque restrains the Kerr effect to the superficial layers of the PC. As a consequence, the slope of the transmission curve on the red side of the bandgap becomes less abrupt. So, unlike what was expected from the linear experience, the illumination of a Kerr PC does not produce exactly a redshift but a deformation of the transmission curve. The bottom of the curve remains fixed as the intensity increases while the upper part of the curve shifts toward the red. Meanwhile the edges' slopes of the bandgap change, becoming steeper on the blue side and gentler on the red side. This difference in slope evolution is of interest for future application as it appears that the blue edge is far more suited for efficient switching than the red one.

Figure 4 maps the evolution of the transmission for a large wavelength domain while the incident intensity varies between a negligible and a high value. For the sake of simplicity, in Fig. 4 we present the *x* axis as an arbitrary unit for an intensity varying between 0 and 1. Without the bistability, Fig. 4 would be symmetric with respect to the median axis. This figure contains 313×21 points, each one being the result of an iterative process applied to the (wavelength, intensity) couple characterizing the point position on the figure. This calculation was made using MATLAB 6.5 on ten Pentium IV 1.5 GHz processors in one week. Such a brute force approach is usually unnecessary but was adopted to illustrate the speed of the FFF. It must also be said that lowering the convergence criterion of our iterative FFF method gives us accurate transmission values five to ten times faster at the price of a slightly underestimated switching intensity. It is also of interest to know that it is possible to compute directly at any given incident intensity without having to compute at lower intensities: The algorithm is robust enough to converge even in those cases and of course it is faster (ranging between a few seconds and five minutes, depending on the behavior of the PC at a given wavelength and intensity).

Another illustration of the capacities of this code is to reveal with a relatively short computer time (2 h for a 200 point curve) the hysteresis phenomenon linked to the presence of a cubic nonlinear material [see Fig. 5(a)]. We can see in Fig. 5(b) that the number of iterations remains low except when the PC's state switches between opaque and transparent. This switch is linked to a discontinuous change of the electromagnetic field map and in this case several tens of iterations are commonly required. Compare Figs. 2(a) and 2(b), which represent the field on each
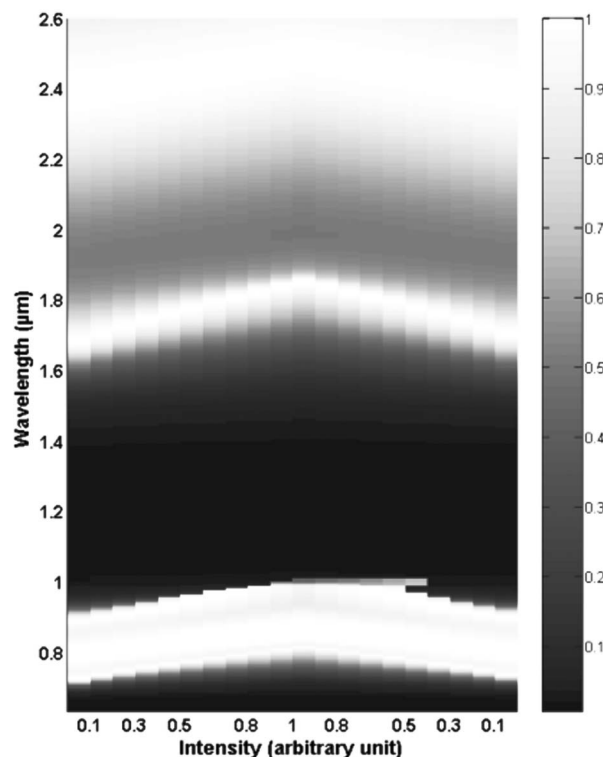

Fig. 4.   Evolution of the transmission map for an increasing value of the magnitude of the incident field.
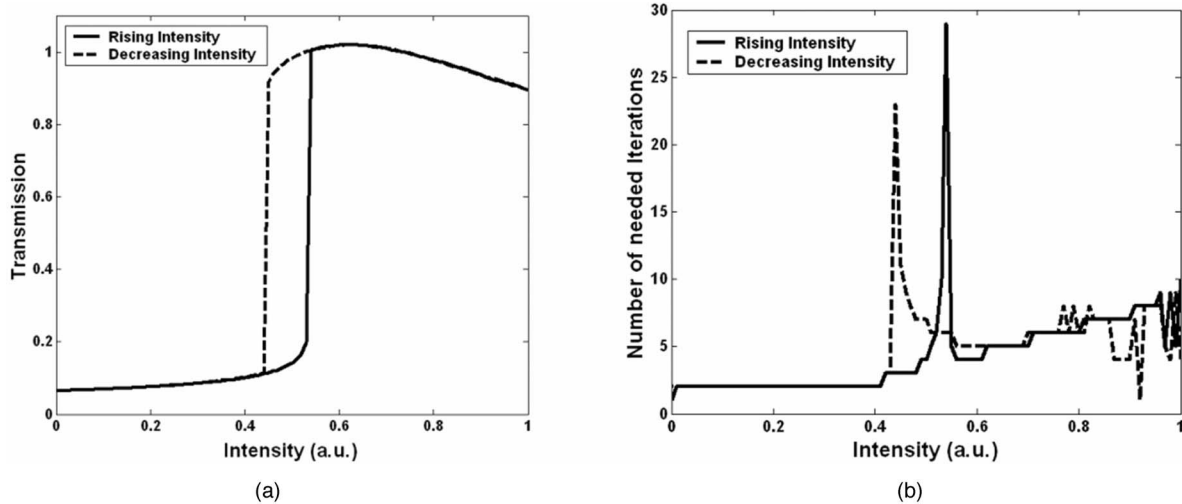
Fig. 5.   (a) and (b) Hysteresis phenomenon obtained at $\lambda = 968$ nm.

side of the rising front discontinuity in Fig. 5(a): The field map has totally changed although the incident intensity has increased only by 1/5000th. The same iteration behavior near the discontinuities was also observed in Ref. 30, although it concerns a thin-film Kerr PC placed inside a Fabry–Perot cavity and not a bulk or thick one standing in air.

5. CONCLUSION

The FFF method when applied to Kerr NPCs is an efficient tool. It is fast and needs few truncated Fourier series coefficients while it is able to cope with high-contrast permittivity structures. Although it is not discussed in this paper, we simulated thick metallic-based PCs at optical wavelengths without any numerical difficulties. Li's inverse rule applied on well-chosen continuous quantities ensuring fast convergence.

The nonlinear effect itself is simulated via an iterative process providing satisfying results if correctly weighted. The results are quickly obtained outside the switching zones, these zones being in the neighborhood of the transmission's discontinuities. Within these zones, the process of nonlinear convergence slows down and needs a careful weighting. It is to be noted that in some rare instances (not shown here), such as small wavelength and high intensity, the iterative process never converges. Careful examination of the iteration process makes us suspect that it is linked to the appearance in the crystal of a multistability behavior different from the regular bistability, although this hypothesis will need further investigation.

The application of our Kerr-based FFF algorithm to the case of the square-lattice 2D PC illustrates the expected redshift occurring with strong illumination of a positive third-order susceptibility material. But we showed that the shift is in reality more complex and results in a deformation of the gap, the bottom of the transmission curve being unmodified while the upper parts shift toward the red. This is a consequence of the penetrating length of the wave inside the PC and produces a difference between the blue and the left side of the bandgap. In the case of a red-

shift (positive $\chi^{(3)}$), the blue side slope becomes steeper with increasing illumination while the red side becomes gentler. The blue side is then more adaptable to a switching application than the red one and they can no longer be considered as equivalent.

Another important point of our FFF-based Kerr algorithm is that the inhomogeneities arising in the originally homogeneous permittivities of the PC nonlinear inclusions are perfectly taken into account. There are other methods, such as the multiple-scattering method, that have to rely on a homogeneous field approximation while coping with such a Kerr simulation.[32] We will reveal in a subsequent paper the limitations and artifacts linked to such an approximation.

J. J. Bonnefois can be reached by e-mail at Jean-Jacques.Bonnefois@u-paris10.fr.

REFERENCES

1. J. Joannopoulos, *Photonic Crystals, Molding the Flow of Light* (Princeton U. Press, 1995).
2. E. Yablonovitch, "Inhibited spontaneous emission in solid-state physics and electronics," Phys. Rev. Lett. **58**, 2059–2062 (1987).
3. A. Priou and T. Itoh, eds., *Progress in Electromagnetic Research* (Universita di Pisa, 2004), Vol. 43.
4. K. Bush and S. John, "Liquid crystal photonic-band-gap materials: the tunable electromagnetic vacuum," Phys. Rev. Lett. **83**, 967–970 (1999).
5. D. Scrymgeour, N. Malkova, S. Kim, and V. Gopalan, "Electro-optic control of the superprism effect in photonic crystals," Appl. Phys. Lett. **82**, 3176–3178 (2003).
6. P. Halevi and F. R. Mendieta, "Tunable photonic crystals with semiconducting constituents," Phys. Rev. Lett. **85**, 1875–1878 (2000).
7. W. Chen and D. L. Mills, "Gap solitons and the nonlinear optical response of superlattices," Phys. Rev. Lett. **58**, 160–163 (1987).
8. S. John and N. Akozbek, "Nonlinear optical solitary waves in a photonic band gap," Phys. Rev. Lett. **71**, 1168–1171 (1993).
9. M. Scarola, J. P. Dowling, C. M. Bowden, and M. J. Bloemer, "Optical limiting and switching of ultrashort

pulses in nonlinear photonic bandgap material," Phys. Rev. Lett. **73**, 1368–1371 (1994).

10. H. Y. Ryu and M. Notomi, "Finite-difference time-domain investigation of band-edge resonant modes in finite-size two-dimensional photonic crystal slab," Phys. Rev. B **68**, 5209–5217 (2003).

11. H. M. Gibbs, *Optical Bistability: Controlling Light with Light* (Academic, 1985).

12. R. Wang, J. Dong, and D. Y. Xing, "Dispersive optical bistability in one-dimensional doped photonic band gap structure," Phys. Rev. E **55**, 6301–6304 (1997).

13. V. Lousse and J. P. Vigneron, "Bistable behaviour of a photonic crystal nonlinear cavity," Physica B **338**, 171–177 (2003).

14. E. Lidorikis, Q. Li, and C. M. Soukoulis, "Wave propagation in nonlinear multilayer structures," Phys. Rev. B **54**, 10249–10252 (1996).

15. N. Akozbek and S. John, "Optical solitary waves in two and three-dimensional nonlinear photonic band-gap structures," Phys. Rev. E **57**, 2287–2319 (1998).

16. S. F. Mingaleev and Y. S. Kivshar, "Self-trapping and stable localized modes in nonlinear photonic crystals," Phys. Rev. Lett. **86**, 5474–5477 (2001).

17. S. Pereira, P. Chark, and J. E. Sipe, "Gap-soliton switching in short microresonator structures," J. Opt. Soc. Am. B **19**, 2191–2202 (2002).

18. P. Xie, Z. Q. Zhang, and X. Zhang, "Gap solitons and soliton trains in finite-size two-dimensional periodic and quasiperiodic photonic crystals," Phys. Rev. E **67**, 026607–026612 (2003).

19. A. M. Kamtchatnoc, S. A. Darmanyan, and M. Nevière, "Polariton gap solitary waves in semiconductor microcavities," J. Lumin. **110**, 373–377 (2004).

20. P. Tran, "Optical limiting and switching of short pulses by use of a nonlinear photonic bandgap structure with a defect," J. Opt. Soc. Am. B **14**, 2589–2595 (1997).

21. L. Brzozowski and E. H. Sargent, "Nonlinear distributed-feedback structures as passive optical limiters," J. Opt. Soc. Am. B **17**, 1360–1365 (2000).

22. B. Y. Soon, J. W. Haus, M. Scalora, and C. Sibilia, "One-dimensional photonic crystal limiter," Opt. Express **11**, 2007–2018 (2003).

23. V. Lousse and J. P. Vigneron, "Self-consistent photonic band structure of dielectric superlattices containing nonlinear optical material," Phys. Rev. E **63**, 027602–027606 (2001).

24. M. Soljacic, M. Ibanescu, S. G. Johnson, Y. Fink, and J. D. Joannopoulos, "Optimal bistable switching in nonlinear photonic crystal," Phys. Rev. E **66**, 055601–055605 (2002).

25. E. Popov and M. Nevière, *Light Propagation in Periodic Media* (Marcel Dekker, 2003).

26. E. Popov and M. Nevière, "Grating theory: new equations in Fourier space leading to fast converging results for TM polarization," J. Opt. Soc. Am. A **17**, 1773–1784 (2000).

27. L. Li, "Use of Fourier series in the analysis of discontinuous periodic structures," J. Opt. Soc. Am. A **13**, 1870–1876 (1996).

28. N. Bonod, E. Popov, and M. Neviere, "Fourier factorization of nonlinear Maxwell equations in periodic media: application to the optical Kerr effect," Opt. Commun. **244**, 389–398 (2005).

29. P. Vincent, N. Paraire, M. Nevière, A. Koster, and R. Reinisch, "Gratings in nonlinear optics and optical bistability," J. Opt. Soc. Am. B **2**, 1106–1116 (1985).

30. V. Lousse and J. P. Vigneron, "Use of Fano resonances for bistable optical transfer through photonic crystals films," Phys. Rev. B **69**, 155106–155117 (2004).

31. D. Felbacq, G. Tayeb, and D. Maystre, "Scattering by a random set of parallel cylinders," J. Opt. Soc. Am. A **11**, 2526–2534 (1994).

32. E. Centeno and D. Felbacq, "Optical bistability in finite-size nonlinear bidimensional photonic crystals doped by a microcavity," Phys. Rev. B **62**, 7683–7686 (2000).